Direct-write assembly of microperiodic planar and spanning ITO microelectrodes†

Bok Yeop Ahn,[ab] David J. Lorang,[ab] Eric B. Duoss‡[ab] and Jennifer A. Lewis*[abc]

Received 1st June 2010, Accepted 7th August 2010
DOI: 10.1039/c0cc01691h

Printed Sn-doped In_2O_3 (ITO) microelectrodes are fabricated by direct-write assembly of sol–gel inks with varying concentration. This maskless, non-lithographic approach provides a facile route to patterning transparent conductive features in planar arrays and spanning architectures.

Printed electronic devices are finding widespread application in thin film transistors,[1] solar cells,[2] batteries,[3] displays,[4] and radio frequency identification (RFID) tags.[5] Common printing techniques, such as ink jet, roll-to-roll, and screen printing, allow only supported, planar structures to be produced. Recently, Ahn *et al.* reported omnidirectional printing of flexible, stretchable, and spanning silver microelectrodes.[6] Here, we demonstrate direct-write assembly of transparent microelectrodes composed of Sn-doped indium oxide (ITO), a widely used conductor in optoelectronic devices.

Direct-write assembly is a maskless, non-lithographic route for patterning planar and three-dimensional (3D) structures.[7–9] In this printing method, a concentrated ink is extruded through a tapered cylindrical nozzle that is translated using a three-axis (x–y–z), robotic motion stage (Fig. 1a). To date, myriad materials, including metallic,[6] polymer,[8] and ceramic[9] inks, have been patterned by this filamentary printing approach. Concentrated inks are typically desired to avoid significant spreading[10] and inhomogeneous drying effects[11] that occur in droplet-based approaches, such as ink-jet printing.

To pattern planar and spanning transparent microelectrodes with fine features ($\leq$5 μm), we developed concentrated sol–gel inks of varying solids loadings. Each ink is produced by first dissolving indium acetate and tin bis(acetylacetonate) dichloride in acetylacetone solvent at 90 °C on a hot plate. The In and Sn precursors are not soluble in alcohol or water, thus acetylacetone is used to both promote their solubility and chelation. Next, an aqueous solution (25 wt%) of tetramethylammonium hydroxide is added drop-wise to each solution, followed by concentrating it to a high solids loading (up to 30 wt%) *via* solvent evaporation at 120 °C. During this step, an aqueous solution (35 wt%) of hydrogen peroxide with a molar ratio of H_2O_2/In > 5 is added in a dropwise manner to accelerate oxidation and suppress recrystallization. Upon cooling to room temperature, a viscous, reddish yellow, transparent ink is obtained (Fig. 1b), which is stable for several months without a noticeable change in printing behavior. More details are given in the ESI.†

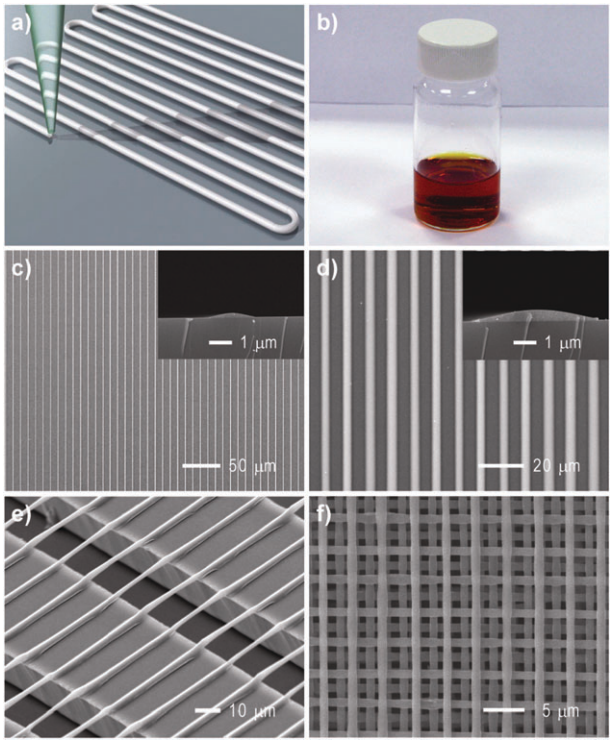

Fig. 1 (a) Schematic illustration of direct-write assembly. (b) Optical image of a representative sol–gel ink. (c) and (d) SEM micrographs of 1D planar array of ITO microelectrodes patterned on a Si wafer using either a 1 μm or 4 μm nozzle, respectively. The insets show cross-section images of the printed and annealed features. (e) SEM micrograph of spanning ITO microelectrodes printed on Si ribbons. (f) SEM micrograph of an as-patterned 3D structure (8 layers).

To demonstrate direct writing of planar arrays, we printed a sol–gel ink (25 wt% solids) on a Si wafer through a 1 μm nozzle (pressure = 25 psi, speed = 500 μm s^{-1}, center-to-center rod spacing = 8 μm). A 1D planar array of ITO microelectrodes is patterned and annealed at 570 °C in air (Fig. 1c). After annealing, the resulting ITO microelectrodes are 1.9 μm in width (w) and 210 nm in height (h) (Fig. 1c, inset). Another 1D planar array is printed through a 4 μm nozzle (pressure = 5 psi, speed = 500 μm s^{-1}) using the same ink (Fig. 1d). After annealing, ITO microelectrodes of

[a] *Department of Materials Science and Engineering, University of Illinois at Urbana-Champaign, Urbana, Illinois 61801, USA. E-mail: jalewis@illinois.edu; Fax: +1 217-333-2736; Tel: +1 217-244-4973*
[b] *Frederick Seitz Materials Research Laboratory, University of Illinois at Urbana-Champaign, Urbana, Illinois 61801, USA*
[c] *Department of Chemistry and Biomolecular Engineering, University of Illinois at Urbana-Champaign, Urbana, Illinois 61801, USA*
† Electronic supplementary information (ESI) available: Experimental details. See DOI: 10.1039/c0cc01691h
‡ Now at the Center for Micro- and Nanotechnology, Lawrence Livermore National Laboratory, Livermore, California, 94551, USA

w = 5.4 μm, h = 510 nm are obtained (Fig. 1d, inset). Their morphology reveals that the ink exhibits only modest lateral spreading on the underlying substrate, since the feature width is roughly twice the nozzle diameter. During annealing, the printed features are constrained by the underlying substrate. Thus, the volumetric shrinkage (~75%) that arises from organic removal and crystallization is accommodated solely by a reduction in height, resulting in planar ITO microelectrodes with an aspect ratio (h/w) of approximately 0.1.

To demonstrate direct writing of spanning microelectrodes, we printed a slightly more concentrated sol–gel ink (28 wt% solids) through a 2 μm nozzle (pressure = 50 psi, speed = 200 μm s^{-1}, center-to-center electrode spacing = 12 μm) on a substrate composed of parallel rectangular Si microribbons (width = 45 μm, height = 26 μm, center-to-center spacing = 70 μm). The Si microribbon array is prepared by a lithographic and etching process.[6,12] Self-supporting ITO microelectrodes that span gaps of ~25 μm are readily obtained upon annealing at 570 °C in air (see Fig. 1e). These conductive features are able to both span gaps across the underlying microribbons as well as retain their nearly cylindrical morphology during printing and annealing. Notably, ITO microelectrodes with $h/w \approx 1$ are produced in a single-pass by this method.

To further demonstrate the assembly of spanning features, we printed 3D microperiodic arrays (Fig. 1f) from the same ink (28 wt% solids) on a Si wafer using a 1 μm nozzle (pressure = 95 psi, speed = 400 μm s^{-1}, center-to-center rod spacing = 4 μm). The rods (w = 1.0 μm) bond to one another and span gaps present in the underlying layers. Again, nearly cylindrical features are observed in each layer.

Control over the ink viscosity and elastic modulus is critical for achieving the printed architectures shown in Fig. 1. The ink viscosity depends strongly on its solids loading. For example, the apparent viscosity of a 5 wt% solids ink is ~0.01 Pa s. However, the ink viscosity increases by four orders of magnitude at a solids loading of 28 wt% (Fig. 2a). Importantly, a modest increase in ink solids loading from 25% to 28% results in nearly a two-order of magnitude increase in apparent viscosity (Fig. 2a), which translates to an order of magnitude difference between the aspect ratios of their respective patterned and annealed features (Fig. 1c and e). During printing, the ink begins to dry immediately as it exits the nozzle, which leads to a concomitant rise in its elastic (G') modulus (Fig. 2b). Unlike the data shown, the printed microelectrodes are expected to undergo solidification ($G' > G''$) on a much faster timescale (~10 ms)[13] due to their vastly higher surface area-to-volume ratio.

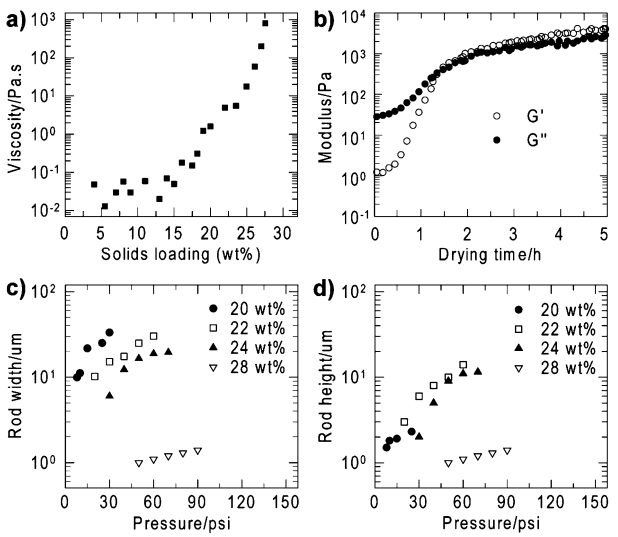

Fig. 2 (a) Apparent viscosity of sol–gel inks as a function of solids loading at a shear rate of 10 s^{-1}. (b) Shear elastic (G') and viscous (G'') moduli of a 25 wt% sol–gel ink as a function of drying time at room temperature. (c) and (d) Rod width and height as a function of applied pressure for as-printed features deposited from inks of varying solids loading.

To further quantify the relationship between ink rheology and printed feature morphology, we measured the printed rod width (w) and height (h) for inks of varying solids loading deposited through a 1 μm nozzle at different applied pressures (Fig. 2c and d). At a constant printing speed of 500 μm s^{-1}, the printed feature width and height increase as the applied pressure increases from 5 to 90 psi. As expected, the minimum pressure required for ink flow increases with increasing solids loading. For example, inks with 20 wt% solids flow through a 1 μm nozzle at applied pressures as low as 5 psi, yielding printed features of w = 10 μm, h = 1.2 μm. Upon increasing the applied pressure to 30 psi, printed features of w = 33.2 μm, h = 2.5 μm are obtained as a result of over pumping. Due to the lower viscosity of this ink, lateral spreading gives rise to features with a low aspect ratio (h/w) ≈ 0.08, which would decrease further upon annealing. Similarly, the widths of features printed from inks with solids loading of 22–28% increase as the applied pressure increases. However, lateral spreading is significantly reduced due to their increased viscosity and shear elastic modulus. For example, inks with 28 wt% solids require a minimum deposition pressure as high as 50 psi to initiate flow, and yield printed features of w = 1.10 μm, h = 1.05 μm at this pressure, with aspect ratio ~0.95. Rapid solidification of these highly concentrated inks enables printing of fine spanning features with nearly cylindrical morphologies.

During thermal annealing of a representative ink (25 wt% solids) in air, significant weight loss occurs followed by crystallization (Fig. 3a and b). First, solvent evaporation occurs at temperatures below ~150 °C, followed by organic decomposition at higher temperatures yielding the desired metal oxide.[14] Thermogravimetric analysis (TGA) indicates that approximately 63 wt% mass loss occurs by 350 °C (Fig. 3a), while X-ray diffraction (XRD) reveals that the onset crystallization occurs by 350 °C (Fig. 3b). All peaks are assigned to In_2O_3,[15] and their intensities increase with increasing temperature. Fig. 3c shows the resistivity (ρ) of ITO thin films (thickness = 150 nm), spin coated from inks containing various tin concentrations and annealed at 570 °C in air, followed by reductive post-annealing in flowing N_2. Reductive post-annealing results in a one order of magnitude decrease in resistivity.[16] Resistivity of these films decreases with increasing tin concentration, attaining a minimum value of 2.4 × 10^{-3} Ω cm at Sn/In = 0.06. The resistivity increase at excess tin concentration is likely due to the deposition of SnO_2 in the

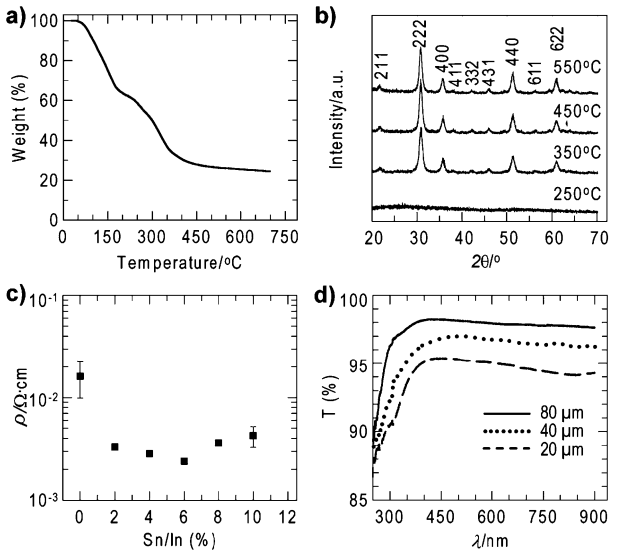

Fig. 3 (a) Thermogravimetric analysis of the ITO ink in air. (b) X-Ray diffraction patterns obtained upon calcining the ITO ink to different temperatures. (c) Resistivity of the ITO thin films coated on a glass substrate. (d) Transmittance of 1D planar arrays of ITO microelectrodes of varying center-to-center spacing patterned on glass substrates.

grain boundaries of In_2O_3.[17] Although this minimum resistivity value is in good accord with those reported for other solution-based ITO films,[18] it is about an order of magnitude higher than the lowest reported values in the literature.[19] Further optimization of the ink formulation and annealing conditions is now underway to improve electrical performance. Fig. 3d shows the optical transmittance of 1D arrays of ITO microelectrodes (w = 2 μm, h = 200 nm) as a function of their center-to-center spacing. Transmittance (T) of patterned microelectrode arrays with 20 μm spacing is as high as 94% in the visible to near infrared region, and increases to 98% as the spacing between ITO microelectrodes increases to 80 μm.

In conclusion, we have demonstrated that planar and spanning ITO microelectrodes can be patterned in both 1D and 3D arrays by direct-write assembly of a concentrated sol–gel ink. Our approach may open new avenues for fabricating printed electronic and optoelectronic devices in unusual layouts.

The patterning work was supported by the DOE Energy Frontier Research Center on Light-Material Interactions in Energy Conversion (Award No. DE-SC0001293) and the ink development was supported by the DOE Programming Function *via* Soft Materials Cluster (Award No. DEFG-02-07ER46471), through the Frederick Seitz Materials Research Laboratory (FSMRL). We gratefully acknowledge use of the FSMRL Center for Microanalysis of Materials at the University of Illinois at Urbana-Champaign. The author B. Y. Ahn thanks the Korea Research Foundation for support in the form of a postdoctoral fellowship. We thank M. J. Motala, R. G. Nuzzo, and J. A. Rogers for providing us with the Si microribbon substrates.

Notes and references

1 H. Sirringhaus, T. Kawase, R. H. Friend, T. Shimoda, M. Inbasekaran, W. Wu and E. P. Woo, *Science*, 2000, **290**, 2123; D.-H. Lee, Y.-J. Chang, G. S. Herman and C.-H. Chang, *Adv. Mater.*, 2007, **19**, 843.
2 C. N. Hoth, S. A. Choulis, P. Schilinsky and C. J. Brabec, *Adv. Mater.*, 2007, **19**, 3973; J. Yoon, A. J. Baca, S.-I. Park, P. Elvikis, J. B. Geddes III, L. Li, R. H. Kim, J. Xiao, S. Wang, T.-H. Kim, M. J. Motala, B. Y. Ahn, E. B. Duoss, J. A. Lewis, R. G. Nuzzo, P. M. Ferreira, Y. Huang, A. Rockett and J. A. Rogers, *Nat. Mater.*, 2008, **7**, 907; X. Guo, H. Li, B. Y. Ahn, E. B. Duoss, K. J. Hsia, J. A. Lewis and R. G. Nuzzo, *Proc. Natl. Acad. Sci. U. S. A.*, 2009, **106**, 20149.
3 L. Hu, J. W. Choi, Y. Yang, S. Jeong, F. L. Mantia, L.-F. Cui and Y. Cui, *Proc. Natl. Acad. Sci. U. S. A.*, 2009, **106**, 21490.
4 B. Comiskey, J. D. Albert, H. Yoshizawa and J. Jacobson, *Nature*, 1998, **394**, 253.
5 V. Subramanian, J. M. J. Frechet, P. C. Chang, D. C. Huang, J. B. Lee, S. E. Molesa, A. R. Murphy, D. R. Redinger and S. K. Volkman, *Proc. IEEE*, 2005, **93**, 1330.
6 B. Y. Ahn, E. B. Duoss, M. J. Motala, X. Guo, S.-I. Park, Y. Xiong, J. Yoon, R. G. Nuzzo, J. A. Rogers and J. A. Lewis, *Science*, 2009, **323**, 1590.
7 J. A. Lewis and G. M. Gratson, *Mater. Today (Oxford, UK)*, 2004, **4**, 32; J. E. Smay, J. Cesarano III and J. A. Lewis, *Langmuir*, 2002, **18**, 5429; Q. Li and J. A. Lewis, *Adv. Mater.*, 2003, **15**, 1639.
8 D. Therriaults, S. R. White and J. A. Lewis, *Nat. Mater.*, 2003, **2**, 265; C. J. Hansen, W. Wu, K. S. Toohey, N. R. Sottos, S. R. White and J. A. Lewis, *Adv. Mater.*, 2009, **21**, 4143; G. M. Gratson, M. Xu and J. A. Lewis, *Nature*, 2004, **428**, 386.
9 J. E. Smay, G. M. Gratson, R. F. Shepherd, J. Cesarano III and J. A. Lewis, *Adv. Mater.*, 2002, **14**, 1279; J. A. Lewis, J. E. Smay, J. Stuecker and J. Cesarano, *J. Am. Ceram. Soc.*, 2006, **89**, 3599.
10 S. B. Fuller, E. J. Wilhelm and J. M. Jacobson, *J. Microelectromech. Syst.*, 2002, **11**, 54; T. H. J. van Osch, J. Perelaer, A. W. M. de Laat and U. S. Schubert, *Adv. Mater.*, 2008, **20**, 343.
11 D. Kim, S. Jeong, B. K. Park and J. Moon, *Appl. Phys. Lett.*, 2006, **89**, 264101.
12 A. J. Baca, M. A. Meitl, H. C. Ko, S. Mack, H.-S. Kim, J. Dong, P. M. Ferreira and J. A. Rogers, *Adv. Funct. Mater.*, 2007, **17**, 3051; D.-Y. Khang, H. Jiang, Y. Huang and J. A. Rogers, *Science*, 2006, **311**, 208.
13 E. B. Duoss, M. Twardowski and J. A. Lewis, *Adv. Mater.*, 2007, **19**, 3485.
14 L. L. Hench and J. K. West, *Chem. Rev.*, 1990, **90**, 33.
15 T. Tsuchiya, H. Niino, A. Yabe, I. Yamaguchi, T. Manabe, T. Kumagai and S. Mizuta, *Appl. Surf. Sci.*, 2002, **197–198**, 512.
16 Y. Takahashi, S. Okada, R. B. H. Tahar, K. Nakano, T. Ban and Y. Ohya, *J. Non-Cryst. Solids*, 1997, **218**, 129.
17 T. Furusaki, K. Kodaira, M. Yamamoto, S. Shimada and T. Matsushita, *Mater. Res. Bull.*, 1986, **21**, 803.
18 R. B. H. Tahar, T. Ban, Y. Ohya and Y. Takahashi, *J. Appl. Phys.*, 1998, **83**, 2631.
19 S. Seki, Y. Sawada and T. Nishide, *Thin Solid Films*, 2001, **388**, 22; R. B. H. Tahar, T. Ban, Y. Ohya and Y. Takahashi, *J. Appl. Phys.*, 1998, **83**, 2139.

